Effects of moving contact line on filament pinch-off dynamics of viscoelastic surfactant fluids

Shijian Wu and Hadi Mohammadigoushki*
Department of Chemical and Biomedical Engineering, FAMU-FSU College of Engineering, Florida State University, Tallahassee, Florida 32310, USA

(Received 18 December 2019; accepted 30 April 2020; published 29 May 2020)

Many practical applications (e.g., coating, painting, printing, or agrochemical spraying) involve depositing complex fluids onto a solid substrate using a predominantly uniaxial extensional flow. In this work, we conduct experiments by gradually depositing non-Newtonian surfactant fluids onto a horizontal solid substrate via a vertical needle. We investigate the extent to which, the spreading dynamics of the fluid contact line on the solid substrate can affect the thinning dynamics of the fluid filament formed between the needle and the substrate. Our work considers two model viscoelastic surfactant fluids based on cetylpyridinium chloride and sodium salicylate (CPyCl/NaSal) and octadecyltrimethylammonium bromide and sodium oleate (C_8TAB/NaOA) in deionized water. Experiments are performed using two flat substrates: a big substrate, where fluid contact line is free to move, and a finite-size substrate, where fluid contact line is pinned. The fluid wetting on the substrate is characterized by measuring the contact-line velocity and dynamic contact angle, while the extensional flow is evaluated by measuring the fluid midfilament diameter. Two novel regimes are identified: In regime I, fluid wetting and filament pinch-off dynamics are independent, while in regime II, the fluid wetting significantly affects the extensional flows by lowering the material extensional relaxation times and Trouton ratios. Our analysis shows that spreading of these viscoelastic surfactant fluids are surprisingly well captured by Tanner's law suggested for spreading of a Newtonian fluid on solid substrates. Finally, we propose a scaling analysis based on a combination of the wetting forces and viscous dissipation that can successfully explain the effects of wetting on filament pinch-off dynamics.

DOI: 10.1103/PhysRevFluids.5.053303

I. INTRODUCTION AND BACKGROUND

The phenomenon of fluid spreading on solid substrates is important in several applications such as inkject printing, gravure printing, contact drop dispensing, shampoos, agrochemical spraying, oil-recovery, coating, and others [1–4]. Good spreading is required for most of these applications. Surfactants are amphiphilic molecules that promote wetting and spreading. Hence, in many of the above applications where wetting of the fluid is desirable, surfactants are added at moderately high concentrations to improve spreading. When dissolved in aqueous medium, surfactant molecules self-assemble into variety of shapes including spherical, rodlike, or lamella depending on the surfactant packing parameter $p = v/a_0 l_c$, where v and l_c are volume and length of the hydrophobic tail and a_0 is area of the hydrophilic head. For $p < 1/2$, surfactants form entangled threadlike micelles in the semidilute regime [5]. In the semidilute concentration regime, self-assembled surfactant solutions exhibit strong shear thinning viscoelastic properties [6–8].

*hadi.moham@fsu.edu

In majority of the above applications, particularly gravure printing and contact drop dispensing, a complex fluid is deposited onto a substrate using a predominantly uniaxial extensional flow. After fluid has touched the solid surface, the fluid contact line will be freely moving, while a fluid column forms in the space between the nozzle and the horizontal surface. This gives rise to an interesting fluid mechanic problem, whereby the fluid filament thinning and wetting dynamics are coupled. On the one hand, formation of such filaments may affect the fluid spreading dynamics on the substrate; on the other hand, a moving fluid contact line may affect the pinch-off dynamics of the filament.

Filament pinch-off dynamics and extensional flows of semidilute viscoelastic surfactant solutions have been extensively studied via capillary breakup extensional rheometry (CaBER) [9–13] or filament stretching extensional rheometry (FiSER) [14,15]. These techniques have provided important new insights about the dynamics of viscoelastic surfactant fluids in primarily extensional flows. For example, the uniaxial extensional flows of viscoelastic surfactant fluids is known to be dominated by strong nonlinear effects such as flow-induced micellar structures [11,12,16] or flow-induced micellar breakage [13,17,18]. These insights are crucial for quantitative analysis of the flow of viscoelastic surfactant solutions through microfluidic cross-slot [19–21], entrance channels [22], flow past a cylinder [23–25], or flow past a falling sphere [17,18,26–28].

The hydrodynamics of the Newtonian droplet spreading on a flat solid substrate is well-understood and several reviews have been compiled on this topic [1,2,29,30]. However, wetting dynamics of the non-Newtonian fluids on solid substrates has been examined to a smaller degree. The effects of shear thinning, elasticity and shear thickening have been considered in the past. Bonn and colleagues have experimentally studied the effects of shear thinning on wetting dynamics of a rigid polymer solution based on Xanthan gum [31]. These researchers illustrated that when gravity is negligible, the shear thinning slows down the spreading of the fluid compared to that of a Newtonian fluid. Subsequent experiments by Wang and co-workers showed a similar trend for the effect of shear thinning [32].

The effects of normal stresses (or elasticity) on the contact-line motion has been studied by considering constant viscosity elastic (Boger) fluids based on polymer solutions on horizontal flat substrates [31,33,34]. Bonn and coworkers showed that the contact-line motion in Boger fluids is similar to Newtonian liquids. Therefore, elasticity does not seem to change the spreading dynamics of the viscoelastic fluids in those studies. Moreover, other researchers have shown that the shear thickening behavior slightly accelerates the droplet spreading dynamics compared to that of a Newtonian fluid [32,35].

In several industrial applications, including the ones noted above, these two aspects (dynamic wetting and extensional flows) are coupled and therefore, investigating the simultaneous effects of these two factors is necessary for proper optimization of these processes. To the best of our knowledge, an investigation into the interplay between dynamic wetting and extensional flows in viscoelastic surfactant solutions does not exist. On the one hand, in all prior extensional flow measurements with CaBER or FiSER, wetting plays a negligible role because the fluid contact line in such devices is intentionally pinned to the lower substrate. On the other hand, prior relevant studies on wetting and spreading have only considered spreading dynamics of sessile droplets on a horizontal substrate in the absence of any extensional flows that could develop in a vertical fluid column.

The main objective of this paper is to fill this gap by investigating, for the first time, the interplay between kinetics of contact-line motion and the filament pinch-off dynamics in viscoelastic surfactant solutions. In particular, our primary goal is to probe the extent to which, if any, wetting of the non-Newtonian surfactant fluids can affect the extensional deformation of the viscoelastic surfactant fluids. To achieve this, we will utilize a modified CaBER device namely as dripping-onto-substrate (DoS), which has been used to quantify the filament thinning dynamics of a range of dilute polymer solutions [36–41]. In DoS experiments, a fluid sample is slowly forced out of a vertical needle to settle on a solid substrate. Once the fluid droplet reaches the substrate, the droplet will spread on the substrate and as a result, a column of fluid forms in the space between the nozzle and the lower plate, which will thin and eventually pinch off. The filament pinch-off

in this case is controlled by a balance between surface tension, elastic and/or viscous forces. In our opinion, the dripping onto substrate technique provides a suitable platform to investigate the interplay between contact-line wetting and the filament pinch-off dynamics. To evaluate whether contact-line dynamics influence the extensional flow properties of complex fluids, we will use a big hydrophilic substrate that allows for a freely moving contact line during extensional flow measurements. The results of these experiments will be directly compared to data obtained with a pinned contact line on a smaller solid substrate made of a similar material.

II. WETTING THEORY

A. Newtonian fluids

The spreading dynamics of a Newtonian droplet is controlled by a combination of forces including gravity, inertia, capillarity and viscous dissipation. The most celebrated theory for wetting of Newtonian fluids (when gravity and inertia are negligible) is proposed by Tanner [42] as follows:

$$R(t) = \left[\frac{10\sigma}{9B\eta}\left(\frac{4V}{\pi}\right)^3 t\right]^{0.1}, \tag{1}$$

where V, R, σ, B, η, and t denote the droplet volume [m^3], radius of the droplet that is in contact with the solid substrate [m], surface tension [N/m], a constant parameter, the fluid viscosity [Pa s], and the wetting time [s], respectively. In addition, the dynamic contact angle of the Newtonian fluid on solid substrates is given by Hoffman-Voinov-Tanner's law as [43–45]

$$\theta^3 \propto U, \tag{2}$$

where U is the contact-line velocity with the unit of [m/s].

B. Shear thinning

Since surfactant solutions used in this work show strong shear thinning behavior, we briefly describe the theoretical background on the spreading dynamics of non-Newtonian shear thinning fluids on solid substrates. For example, the theoretical work of Starov and coworkers [46] showed that for a power-law fluid with a viscosity of $\eta = K\dot{\gamma}^{n-1}$, where K, $\dot{\gamma}$, and n are consistency factor, shear rate, and the power-law index, respectively, and the spreading radius of a shear thinning axisymmetric droplet in contact with the solid substrate is expressed as

$$R(t) = R_0\left[1 + \frac{n}{2n+1}\frac{\Lambda}{\beta}\left(\frac{\sigma}{K}\right)^{1/n}\frac{V^{(n+2)/n}}{(2\pi)^{(n+2)/n}R_0^{1/\beta}}t\right]^{\beta}, \tag{3}$$

where R_0 is the initial radius of the contact line, Λ is a dimensionless constant, and $\beta = \frac{n}{3n+7}$ is the spreading exponent. Rafai *et al.* [31] have arrived at a similar relation for spreading of shear thinning power-law fluids. For a Newtonian fluid $\beta = 0.1$, which leads to recovery of Tanner's law.

In addition, Starov *et al.* [46] showed that the contact-line velocity U for a power-law fluid can be expressed as

$$U = \frac{\Lambda n}{2n+1}\left(\frac{\sigma}{K}\right)^{\frac{1}{n}}\left(\frac{2\pi}{V}\right)^{\frac{1-n}{3n}}\left(\frac{\theta}{8}\right)^{\frac{2n+7}{3n}}. \tag{4}$$

For Newtonian fluids Eq. (4) yields the Hoffman-Voinov-Tanner's relation [Eq. (2)].

C. Normal stresses

Normal stresses that are developed in the droplet of wormlike micelles, during spreading process, can facilitate the spreading dynamics. Normal stress differences in a viscoelastic fluid can be

expressed as $N_1 = \Psi\dot{\gamma}^2$, where Ψ is the first normal stress difference coefficient. Rafai *et al.* [31] showed that if r is the distance from droplet peripheral, the normal stress gradients in a drop can be estimated as $\nabla N_1 \approx N_1/r$ and the viscous stress gradient is $\eta\dot{R}/h$. Here $\dot{R}$ and h denote the rate of change in contact-line radius and the height of the spreading droplet, respectively. The ratio of these stresses $\mathcal{N} = \frac{\Psi\dot{R}}{\eta r}$ can be used to determine if the normal stresses are significant. At a critical radius of r_c (near the contact-line edge), where the normal stresses start dominating the viscous stresses, Rafai *et al.* [31] showed that the contact-line radius contains a logarithmic correction to Tanner's law and is given by

$$R(t) \sim V^{3/10}\left(\frac{\sigma t}{\eta}\right)^{1/10}\left[\log\frac{\eta t}{10\Psi_1}\right]^{-1/10}. \tag{5}$$

To evaluate the important forces acting on viscoelastic surfactant solutions during droplet spreading in DoS experiments, the above relations [Eqs. (1)–(5)] will be compared to the experimental data.

III. MATERIALS AND METHODS

Experiments are performed on two sets of viscoelastic surfactant fluids: (1) monohydrate cetylpyridinium chloride (CPyCl) and sodium salicylate (NaSal), and (2) octadecyltrimethylammonium bromide (C_8TAB) and sodium oleate (NaOA). Both systems are prepared by mixing the chemicals in deionized water. CPyCl and NaSal are supplied by Sigma-Aldrich. C_8TAB and NaOA are acquired from TCI America. The aqueous solutions of CPyCl/NaSal contain a fixed amount of [CPyCl] = 100 mM and various salt concentrations [NaSal] = 53–90 mM. In addition, the total salt and surfactant concentration in C_8TAB/NaOA solution is 3 wt% (C_8TAB+NaOA) with the relative weight fraction of C_8TAB varying from 25 to 70 wt%.

The primary objective of this study is to systematically investigate the effects of wetting dynamics on extensional rheology of surfactant solutions by modifying the rheological properties (e.g., viscosity and relaxation times) and type of the surfactant and/or salt. One commonly accepted way to modify the rheological properties of surfactant solutions is to change the salt concentration at a fixed surfactant concentration. In doing so, we noticed that majority of surfactant solutions used in literature show a peak in zero-shear-rate viscosity when the salt concentration increases beyond a critical threshold at a fixed surfactant concentration. Overwhelming majority of such studies have suggested two possible mechanisms for existence of the peak in the zero-shear-rate viscosity: (1) transition from linear to branched micelles [47–52] and (2) beyond the critical concentration, micelles shrink in size but retain their linear morphology [53–55]. CPyCl/NaSal is a well-studied system that follows scenario (1), while C_8TAB/NaOA solution serves as the model fluid system for the second scenario. Therefore, these two micellar systems with different salt to surfactant concentration ratio enable us to access a broad range of rheological properties and micellar microstructure.

The steady-state shear rheology response of these solutions were measured in a commercial Anton-Paar rheometer (MCR 302) using a standard bob and cup geometry with $R_i = 13.5$ mm and $R_o = 14.5$, where R_i and R_o denote the radius of the bob and cup, respectively. Moreover, a standard cone-and-plate geometry with a cone diameter of 50 mm and cone angle of 1° was used for normal stress measurements. In these experiments, a range of shear rate is imposed to the solutions and the resulting steady-state shear viscosity and/or normal stress differences are measured. In addition, the small amplitude oscillatory shear experiments were performed to obtain the viscoelastic properties of the wormlike micelles.

Figure 1 shows a schematic of the custom-made dripping onto substrate experiments used in this paper. In this device, we use a syringe pump to inject the fluid in a vertical blunt needle (with an inner diameter of 1.7 mm) at a flow rate of 30 μl/min. The distance between the needle and the solid surface is chosen to be 4 mm, and once the fluid touches the lower substrate, flow is stopped. The

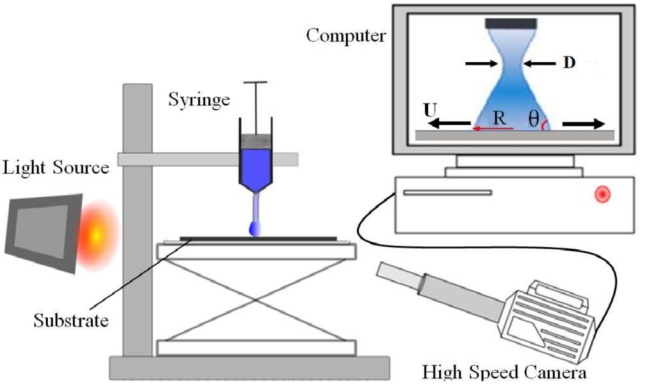

FIG. 1. A schematic of the custom-made dripping onto substrate device that is used to perform experiments in this study. In this figure U, R, θ, and D denote the contact-line velocity, radius of the contact line, contact angle, and the midfilament diameter.

fluid column that forms between the needle and the solid surface will undergo a filament thinning process and eventually pinch off. The solid substrates are disks made of stainless steel with diameter of 10 cm and 4 mm. The smaller size substrate is chosen such that the fluid contact line can be pinned to the edges of the substrate, while, on the larger substrate, the fluid contact line can freely move outwards. After finishing each experiment, we use deionized water to thoroughly clean the surface and dry it before the next experiment. We have reproduced our experiments several times, therefore, this cleaning procedure does not affect the results. A high speed camera (Model Phantom Miro-310, Vision Research Inc.) is used to acquire temporal evolution of the filament thinning and the contact-line dynamics [13].

A MATLAB script has been developed in house to further analyze the raw images acquired by the high speed camera. Through edge detection algorithm we have quantified the temporal evolution of (1) the midfilament diameter, (2) the radius of the droplet that is in contact with the horizontal solid substrate, and (3) the fluid contact angle at the contact line. Further detailed information about our image analysis technique is provided in the Supplemental Material [56].

IV. RESULTS

Figure 2 shows the zero-shear-rate viscosity of the two viscoelastic surfactant solutions as a function of salt to surfactant concentration ratio. It is evident that the zero-shear-rate viscosity in these two solutions exhibit a maximum that is reminiscent of the topological transitions of the micelles reported in previous publications.

Figure 3(a) shows a series of snapshots that illustrate the filament thinning dynamics and contact-line motion for a viscoelastic surfactant solution of CPyCl/NaSal (100 mM/60 mM). In addition, Fig. 3(b) shows a similar solution when the fluid contact line is fixed at the peripheries of the lower surface. For the larger substrate, the contact line is free and moves radially outwards to partially wet the solid surface. This motion leads to further stretching of the elastic fluid filament that is formed between the needle and the solid substrate. Conversely, for the smaller substrate, the contact line is pinned and does not move during filament thinning process and therefore, the length of the fluid filament remains unchanged.

Figure 4 shows the temporal evolution of the dimensionless filament diameter D/D_0 for the two series of viscoelastic surfactant fluids. Here, D and D_0 correspond to the midfilament diameter and the initial fluid filament diameter in DoS experiments, respectively. In Fig. 4, empty symbols correspond to the results of DoS experiments when the fluid contact line is free, while filled symbols denote the experiments for which the fluid contact line is pinned. Clearly, the filament thinning

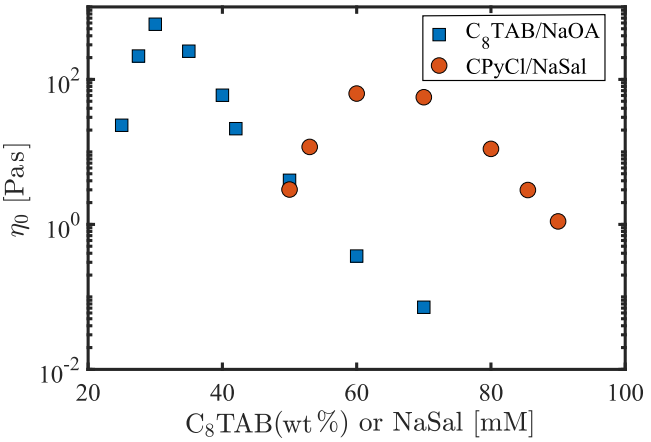

FIG. 2. Zero-shear-rate viscosity of the viscoelastic micellar solutions.

process follows two distinct regimes: For some solutions (e.g., 30% C_8TAB/NaOA or CPyCl/NaSal with [NaSal] = 60 mM), the filament thinning is similar for both free and pinned contact lines (regime I). Whereas, for other solutions (e.g., 50% C_8TAB/NaOA or CPyCl/NaSal with [NaSal] = 53 mM), the filament thinning dynamics are qualitatively different for the free and pinned contact lines (regime II).

Figure 5 illustrates the lifetime of the fluid filaments in these viscoelastic surfactant solutions. Empty symbols denote experiments with the pinned contact line, while filled symbols correspond to a freely moving contact line. In regime I, the filament lifetime for experiments with the free contact line is similar to that of the experiments with the pinned contact line. While in regime II, the filament lifetime for a free contact line is shorter than the experiments with pinned contact line. For experiments with pinned contact line, the filament lifetime is defined as the interval between pinning moment to the filament pinch-off instant. Additionally, for experiments with the big substrate, the filament lifetime is defined from the moment that the diameter of the fluid on the surface is 4 mm until the filament pinch-off time.

We have investigated the effects of the contact-line motion on extensional rheological properties of these systems by calculating the extensional relaxation time and the maximum Trouton ratios.

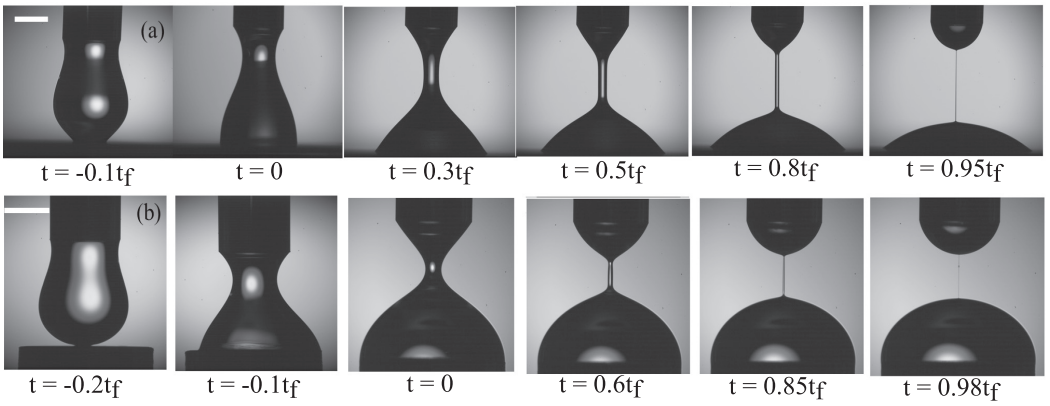

FIG. 3. Filament thinning and contact-line dynamics in a viscoelastic micellar fluid based on CPyCl/NaSal (100 mM/60 mM) when the contact line is (a) free and (b) pinned to the lower plate. The filament pinch-off time is denoted as t_f. The length of the scale bar in panels (a) and (b) is 1.5 mm.

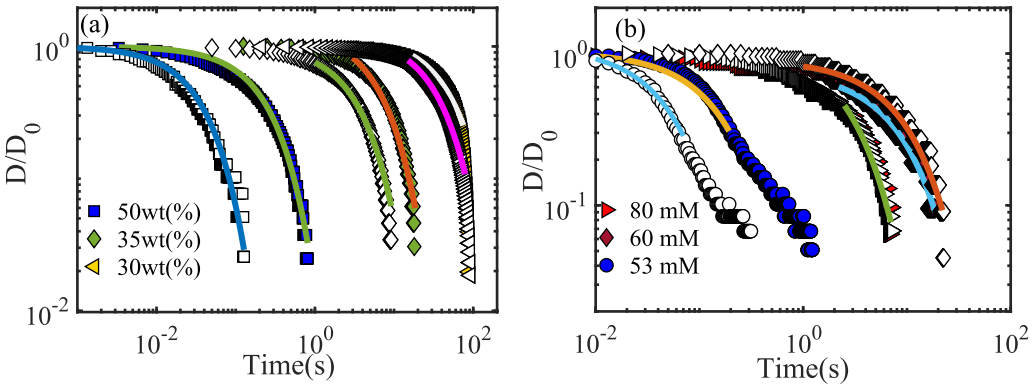

FIG. 4. Time-resolved variation of the dimensionless filament diameter for the two viscolastic surfactant fluids based on (a) C_8TAB/NaOA and (b) CPyCl/NaSal system. The filled symbols denote the results with pinned contact line, while empty symbols correspond to the freely moving contact line. The solid curves correspond to the best fit of Eq. (6) to the elastic regime. The midfilament diameter at the beginning of the experiments is denoted as D_0.

To determine the extensional relaxation times of the viscoelastic surfactant fluids, the exponential relation proposed by Entov and Hinch [57] [Eq. (6)] was fitted to the experimental data in the intermediate elastic regime, where the filament diameter decays exponentially with time (see continuous curves in Fig. 4). To determine the intermediate elastic thinning regime in DoS experiments, the initial and final points of fitting need to be identified. We have shown in our previous published work that the onset of elastic regime is characterized by formation of a cylindrical filament that can be observed in raw images. The end of elastic thinning regime is the time that the transient extensional viscosity reaches an asymptotic value. For further details on the exponential fitting to the experimental data, readers are referred to our earlier study [13]. Figure 6 shows the resulting extensional relaxation times for the two model viscoelastic surfactant fluids. Similar to the two regimes reported for the filament lifetime, we report two regimes for extensional relaxation times. In regime I, the extensional relaxation times obtained for pinned and free contact lines are the same, while in regime II, the extensional relaxation times obtained in experiments with a freely moving contact line are shorter than that of measured for the pinned contact line:

$$\frac{D}{D_0} \propto \exp(-t/3\lambda_E). \tag{6}$$

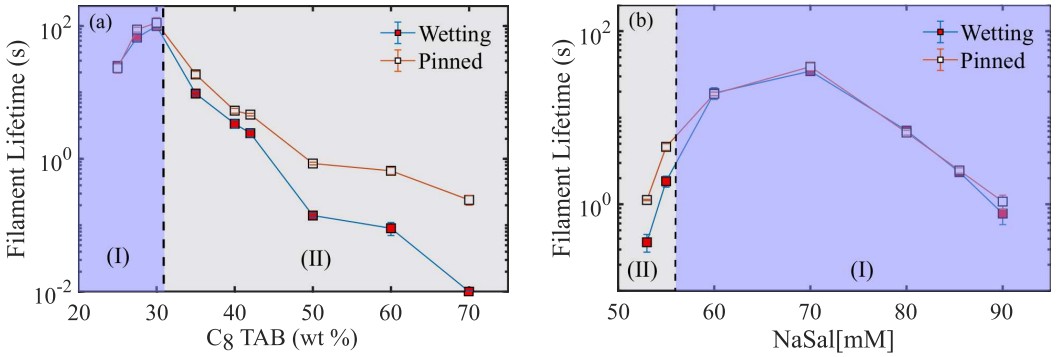

FIG. 5. Filament lifetime as a function of (a) C_8TAB weight percentage for C_8TAB/NaOA viscoelastic solutions and (b) NaSal concentration in the CPyCl/NaSal systems.

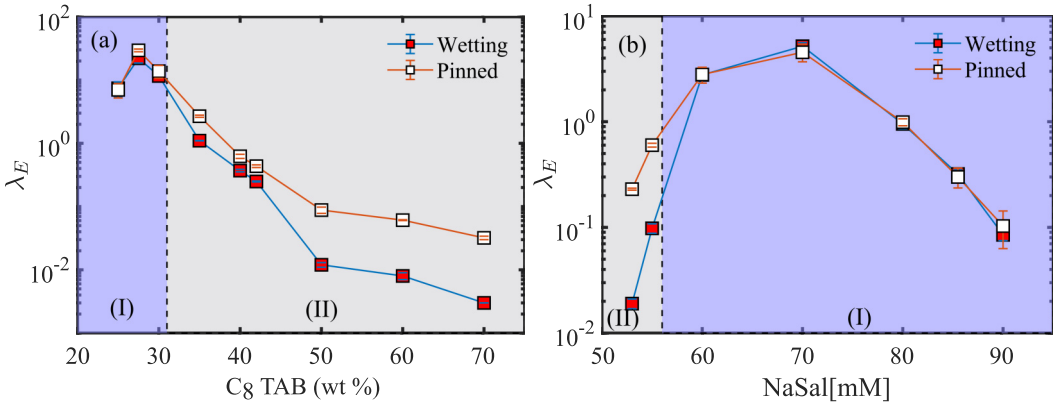

FIG. 6. Extensional relaxation time of the viscoelastic surfactant fluids as determined by the best fit to Eq. (6) for (a) C_8TAB/NaOA and (b) CPyCl/NaSal fluids. Empty symbols correspond to the experiments where contact line is pinned, while, filled symbols correspond to the freely moving contact lines.

Moreover, Fig. 7 shows the maximum Trouton ratio of these viscoelastic systems for pinned and freely moving contact lines. The maximum Trouton ratio is defined as $\mathrm{Tr}_{\max} = \eta_{E,\max}/\eta_0$, where $\eta_{E,\max}$ and η_0 denote the maximum transient extensional viscosity before filament pinch-off moment and the zero-shear-rate viscosity of the fluids. The transient extensional viscosity is defined as $\eta_E = -\sigma/(dD/dt)$, where σ denotes the surface tension of the viscoelastic surfactant solutions. In this study, we used surface tension $\sigma = 32$ mN/m for CPyCl/NaSal and 35 mN/m for C_8TAB/NaOA solutions [13]. The transient extensional viscosity of the viscoelastic surfactant solutions increases as filament undergoes the thinning process and levels off before the filament pinch-off moment (results not shown). This is consistent with prior published studies on viscoelastic surfactant fluids [9,10,13]. Again, the two regimes are observed for the maximum Trouton ratios of these viscoelastic surfactant fluids.

In summary, we report two distinct behavior for extensional flows of these viscoelastic fluids. In regime I, the fluid response does not depend on the dynamics of the contact line (whether free or pinned), while in regime II, a free contact line leads to shorter filament lifetimes, shorter relaxation times and smaller maximum Trouton ratios than that of measured for the pinned contact line. In the following, we will provide a detailed quantitative analysis to rationalize these findings.

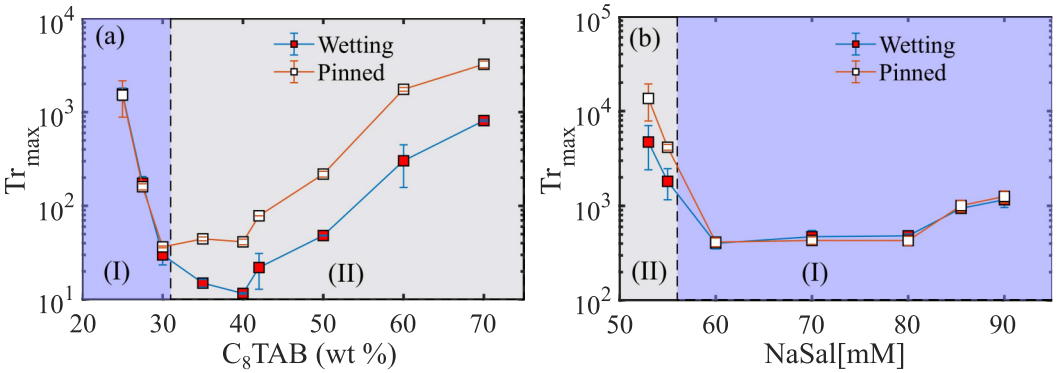

FIG. 7. Maximum Trouton ratio ($\mathrm{Tr}_{\max}$) as a function of salt to surfactant ratios for (a) C_8TAB/NaOA and (b) CPyCl/NaSal viscoelastic fluids. Filled symbols indicate a freely moving contact line, while empty symbols correspond to pinned contact lines.

TABLE I. List of viscoelastic surfactant fluids with their properties.

Fluid	Chemical	Concentration	Bo	α	m_2	m_1	$\dot{\gamma}_{\min}$ (1/s)	$\dot{\gamma}_{\max}$ (1/s)	θ_f
		25 wt%	3.54	0.08	3.4	6.6	0.001	0.16	21.6
		27.5 wt%	3.96	0.09	4.1	5.5	0.001	0.11	35
		30 wt%	5.9	0.08	3.2	10.7	0.0007	0.03	50
		35 wt%	5.4	0.08	3.9	6.8	0.0007	0.02	41.2
C_8TAB/NaOA	C_8TAB	40 wt%	3.75	0.12	3.6	7.4	0.005	0.166	33.5
		42 wt%	3.14	0.13	3.8	6.5	0.032	0.39	36.5
		50 wt%	2.75	0.12	3.8	7.1	0.104	3.41	42.3
		60 wt%	2.41	0.13	3.3	6.1	0.22	5.12	36.2
		70 wt%	2.58	0.13	2.9	4.0	0.31	70	29.5
		53 mM	3.97	0.13	3.4	7.8	0.054	1.23	51
		55 mM	3.62	0.10	3.5	4.9	0.015	0.25	48.5
		60 mM	5.4	0.14	3.8	5.9	0.0023	0.11	43.3
CPyCl/NaSal	NaSal	70 mM	7.66	0.13	2.6	5.7	0.0023	0.12	31.7
		80 mM	4.42	0.15	3.2	6.9	0.015	0.15	39.8
		85.5 mM	3.58	0.18	3.2	5.8	0.02	0.32	55.6
		90 mM	3.14	0.14	2.5	5.3	0.18	2.36	53

V. DISCUSSION

To further elucidate the role of the contact-line motion (i.e., wetting) in DoS experiments, we begin our discussion by evaluating the important forces that control the contact-line dynamics in viscoelastic fluids. When contact line is free, its motion is controlled by a balance between wetting forces on the surface, gravity, inertia, elastic and/or viscous forces. The normal stresses may develop in the bulk of the moving droplet and in the vertical fluid column that forms between the needle and the substrate. While wetting forces, inertia, gravity and normal stresses in the droplet facilitate the droplet spreading, viscous forces inside the droplet and elastic stresses that are developed in the vertical fluid column resist against droplet spreading.

First, to assess the importance of the gravitational forces, we will use dimensionless Bond number defined as $\mathrm{Bo} = 4\rho g R(t)^2/\sigma$, where ρ is the fluid density. Table (I) shows the maximum Bond number for samples tested in these experiments. We note that the contact-line radius increases as a function of time in DoS experiments. Therefore, the maximum Bond number is defined for the conditions that correspond to the filament pinch-off moment. It is clear that the Bond number for all experiments is beyond unity, which indicates that gravity is important in these experiments. An alternative way to evaluate the importance of the gravitational forces is to compare the radius of droplets with that of the capillary length $l = (\sqrt{\sigma/\rho g}) \approx 1.87$ mm. Our experiments indicate that the radius of the contact line for all experiments is larger than the capillary length. Therefore, we conclude that the gravitational forces are important in these experiments.

The effects of inertia is negligible in these experiments because the Reynolds number $Re = \rho U R/\eta \ll 1$. As pointed out in the introduction, the wetting process in both Newtonian and non-Newtonian fluids is described by a universal power-law relation as $R(t) \propto t^{\alpha}$, where α can vary depending upon the type of fluid or forces involved in the wetting process. To assess the significance of the viscous, elastic and surface tension forces in our experiments, we have plotted the temporal evolution of the dimensionless radius of the droplet on the surface as a function of time for different viscoelastic surfactant solutions in Fig. 8(a). We have fitted the data of Fig. 8(a) to such a power law relation. Figure 8(b) shows the power law index α for all fluids considered in this work when the contact-line is free. Interestingly enough, the average value of this power index $\alpha = 0.11 \pm 0.03$, which is very close to the celebrated Tanner's law for Newtonian sessile droplets spreading on a surface in the absence of gravity [42,58–60].

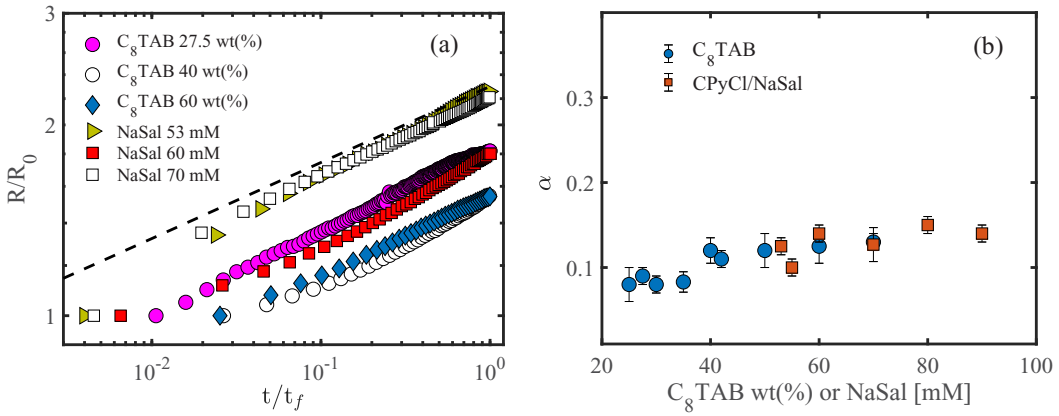

FIG. 8. (a) Dimensionless radius of the contact-line as a function of time for sample viscoelastic surfactant fluids. The dashed curve corresponds to $R(t) \propto t^{\alpha}$ when $\alpha = 0.1$. (b) The power exponent (α) as a function of salt concentrations (NaSal) and surfactant concentration (C_8TAB) in viscoelatic fluids under consideration in this study.

An alternative way to analyze the spreading dynamics of viscoelastic surfactant solutions is to quantify the temporal evolution of the fluid contact angle and contact-line speed. The dynamic contact angle of the spreading droplet is an important parameter that provides a more in-depth understanding of the forces involved in wetting and spreading of the fluids. Figure 9 shows the normalized contact-line velocity U/U_f as a function of the dimensionless dynamic contact angle θ/θ_f for sample surfactant fluids. Here θ_f and U_f denote the dynamic contact angle and the contact-line velocity at the moment of filament pinch-off. The kinetics of the fluid contact angle in Fig. 9 could be divided to two stages denoted by filled and open symbols. Right after the fluid has touched the solid substrate θ/θ_f is at its maximum and the contact angle begins to decay very rapidly [see also, e.g., fluid snapshots for $-0.1t_f < t < 0$ in Fig. 3(a)]. We call this early stage of the wetting and use empty symbols to denote this rapid contact-line wetting process. Based on our visual observations, the end of the early stage of the wetting always coincides with the onset of filament formation [i.e., $t = 0$ in Fig. 3(a)]. Beyond $t = 0$, the contact angle decays with a slower rate toward equilibrium contact angle. We call this the late stage of the wetting [see

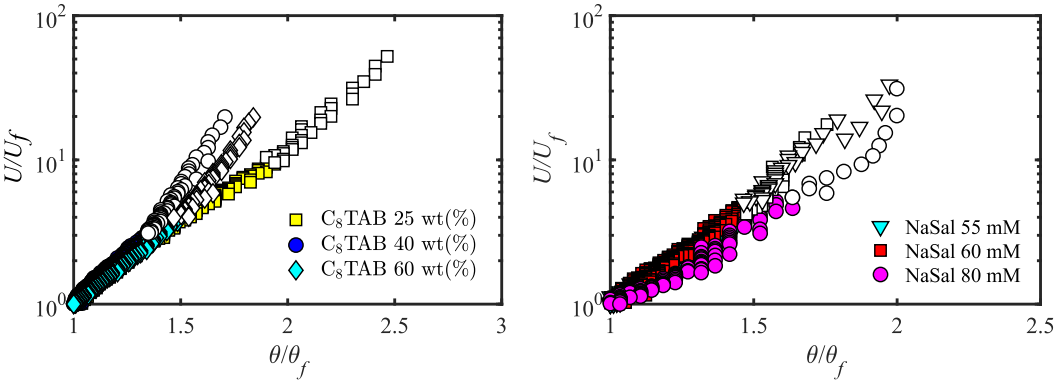

FIG. 9. Dimensionless contact-line velocity as a function of contact angle for viscoelastic surfactant fluids. Empty symbols correspond to the rapid decay of the contact angle after deposition of the fluid onto the solid substrate and filled symbols indicate the contact-line dynamics during extensional flow measurements.

$t = 0 - 0.95t_f$ in Fig. 3(a)] and use filled symbols to mark this regime. The late stage of the wetting always coincides with the time window for which the extensional flow measurements are performed.

To further analyze these results and to identify the important forces that control the contact-line dynamics in these two regimes, the data of Fig. 9 are fitted to the power-law function of $U \sim \theta^m$, and the power-law indices are determined for the early and late stages of the wetting. Table I shows the power-index m for each surfactant solutions. Power-law indices m_1 and m_2 correspond to the early and the late stages of the wetting, respectively. For the early stages of the wetting, $m_1 > 3$, while the late wetting stage is best described with $m_2 \approx 3.3 \pm 0.4$. Based on this analysis, the early stages of the fluid wetting significantly deviate from Tanner-Voinov-Cox relation proposed for Newtonian fluids. This is perhaps not surprising, because as noted by Wang and coworkers, the Tanner-Voinov-Cox relation [Eq. (2)] is valid only for the late time spreading behavior when the contact angle approaches the equilibrium contact angle [61]. Therefore, at the early stages of the wetting, where the contact angle is far from equilibrium, a new model should be developed to better capture the dynamics of spreading and contact-line motion [61]. However, the data of Fig. 9 indicates that in the late stages of the contact-line motion during which extensional flow measurements of Figs. 5–7 are performed, the wetting dynamics closely follow Tanner-Voinov-Cox relation. This clearly confirms that the wetting dynamics of surfactant solutions during extensional flow measurements is controlled by a combination of wetting and viscous forces. This result is consistent with the above discussion on Fig. 8, that during the filament thinning process, the wetting is controlled by capillarity and the viscous forces.

The surfactant solutions considered for this study exhibit a strong shear thinning viscoelastic behavior (see Figs. S2 and S3 in the Supplemental Material [56]). Therefore, it is rather unexpected to observe that shear thinning and normal stresses do not affect the fluid spreading dynamics during extensional flow measurements. To assess the effects of these non-Newtonian features on the spreading dynamics of these surfactant solutions, we have calculated the characteristic shear rate at the fluid contact line for all experiments. The shear rate at the contact line is defined as: $\dot{\gamma} = \frac{1}{R(t)} \frac{dR(t)}{dt}$. This characteristic shear rate is calculated by differentiating a smooth spline function that is fitted to the data of Fig. 8(a). This minimizes the scattering caused by differentiating the raw data (see Fig. S4 in the Supplemental Material [56]). The characteristic shear rate is maximum at the early stages of the wetting process and gradually decays as wetting is underway. Table I shows the minimum and maximum characteristic shear rates that the contact line experiences over the course of filament thinning process. Even the maximum characteristic shear rate for each solution lies below the onset of shear thinning regime in the steady shear viscosity data [compare characteristic shear rates of Table I with the onset of shear thinning in Fig. S2 of the Supplemental Material [56]). This means that these fluids behave Newtonian-like at the contact line and therefore, shear thinning should not affect the dynamics of the contact line.

To assess the effects of bulk normal stresses, we have measured the first normal stress coefficients Ψ_1 as a function of shear rate for the viscoelastic surfactant solutions (see Fig. S5 in the Supplemental Material [56]). The normal stress differences for the range of shear rates shown in Table I are not detectable in the rheometer. In addition, if normal stresses were important, Eq. (5) would have predicted α values smaller than 0.1. Since this is not the case in our experiments, we can conclude that the normal stresses that develop in the bulk of the liquid droplet are unimportant and should not affect the wetting dynamics. In addition to the bulk normal stresses, normal stresses can develop in the vertical fluid filament. These normal stresses act as a resistance against the droplet spreading on the solid substrate and hence, should slow down the wetting dynamics of surfactant solutions. However, as shown in experimental results of Figs. 8 and 9, the spreading dynamics of the wormlike micelles does not appreciably differ from that of a sessile Newtonian droplets (with no vertical fluid filament attached to it). Our hypothesis is that the normal stresses inside the vertical thinning filament, between the needle and the substrate, may have compensated for the effects of gravity. To test this hypothesis, we provide an estimate for the normal stresses in the vertical fluid filament and compare that to the gravitational stresses. The normal stresses in the vertical fluid

column can be estimated as: $\eta_E \dot{\varepsilon}$, where extension rate $\dot{\varepsilon} = \frac{-2}{D(t)} dD(t)/dt$. The ratio of the normal stresses in the vertical fluid column to that of the gravity $\mathcal{E}$ is

$$\mathcal{E} \sim \frac{\eta_E \dot{\varepsilon}}{2\rho g R(t)} \sim \frac{\sigma}{\rho g R(t) D(t)}. \tag{7}$$

During extensional rheological measurements, the midfilament diameter, D and the radius of the contact line, R vary typically from 1 to 0.1 mm and 1.5 to 5 mm, respectively. Using this information, $\mathcal{E}$ is estimated to be in the order of unity, and therefore verifies our hypothesis that the normal stresses that develop in the vertical fluid column balance out the effects of gravitational stresses.

The above analysis together with the experimental results of Figs. 8 and 9 suggest that although these surfactant solutions are strongly shear thinning viscoelastic fluids, their wetting dynamics are controlled only by viscous stresses that develop in the droplet and the capillary forces. In the following we invoke a simple scaling analysis based on the balance between the surface tension forces and the viscous dissipation to assess whether we can distinguish the two regimes reported in Figs. 5–7. During drop spreading, the wetting force, F_w, which is the driving force for spreading is counteracted by the viscous dissipation force, F_v. The balance between these two forces controls the kinetics of wetting. F_w results from surface tension forces and can be expressed as

$$F_w \approx 2\pi R(t) \sigma \cos\theta. \tag{8}$$

However, the viscous dissipation for a Newtonian droplet is

$$F_v \approx \eta \dot{\gamma} \pi R^2(t). \tag{9}$$

By constructing the ratio of these two forces, a capillary number emerges as

$$\mathrm{Ca} = F_v/F_w = \eta U_{\mathrm{ave}}/2\sigma \cos\theta_{\mathrm{ave}}. \tag{10}$$

For the sake of simplicity, we have used an averaged contact-line velocity U_{ave}, contact angle θ_{ave}, and the zero-shear-rate viscosity of the viscoelastic micellar fluids to calculate the capillary numbers for each of the surfactant solutions. The average velocity and the contact angle are determined by taking the arithmetic average of the velocity and/or the contact line at the beginning of the filament formation and right before the filament pinch-off moment. Figure 10 shows the capillary number as a function of concentration for the two viscoelastic surfactant fluids. In this figure, empty symbols denote experiments where the contact-line wetting significantly changes the extensional properties of the fluid (regime II), while filled symbols correspond to the cases that wetting does not affect the extensional rheological properties (regime I). Beyond a critical capillary number Ca $\approx$0.1, the wetting dynamics affect the extensional flow properties of the viscoelastic surfactant fluids. Interestingly enough, this dimensionless capillary number can separate the two regimes from each other and therefore, serves as a suitable criterion to explain the spreading dynamics of these surfactant solutions in DoS experiments.

A simple check for the above criterion is to test its validity for Newtonian fluids. To do so, we have performed DoS experiments on two Newtonian fluids using pinned and freely moving contact lines. Our results indicate that fluid spreading on the solid surface does not affect the filament pinch-off dynamics in these Newtonian fluids (see Fig. S6, Fig. S7, and Table I along with the pertaining discussion in the Supplemental Material [56]). Furthermore, by using a similar procedure described above for viscoelastic surfactant solutions, we have calculated very small capillary numbers for the experiments with these two Newtonian fluids (10^{-3} and 6×10^{-3}). These capillary numbers are well below the critical capillary number of Ca ≈ 0.1 shown in Fig. 10. This result is consistent with the above findings that the contact-line wetting does not affect the filament pinch-off dynamics of these Newtonian fluids. Hence, the criterion based on the capillary number holds for Newtonian fluids. The classical formulation of the advancing contact-line problem in Newtonian fluids with no-slip boundary condition on a solid surface gives rise to the nonintegrable singularity of the shear stress, and fluid pressure at the moving contact line [62]. From a physical

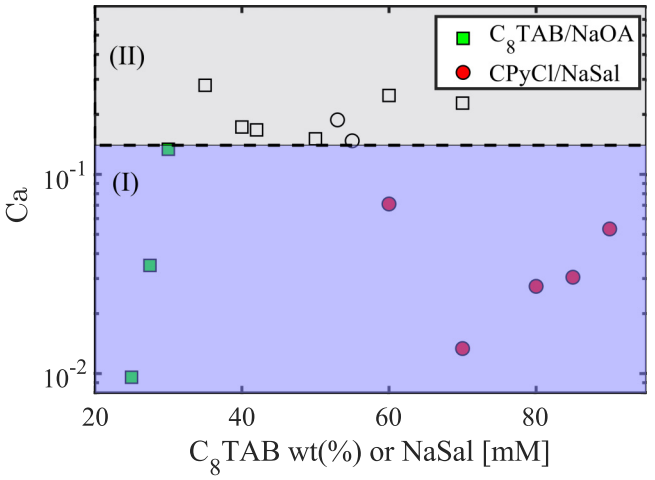

FIG. 10. Capillary number as a function of salt (NaSal) or surfactant (C_8TAB) concentrations for the two viscoelastic surfactant fluids studied in this work. Filled symbols indicate experiments where the contact-line wetting does not influence the extensional flow measurements, while empty symbols are those cases that contact-line dynamics significantly affect the extensional flow properties.

point of view, the singularity problem is not meaningful, therefore, several methods (e.g., replacing the no-slip boundary condition on the solid surface by a slip one [62,63]) are proposed to remove the contact-line singularity. For shear-thinning fluids, calculations have shown that the contact-line singularity is removed due to the viscosity decrease [64,65]. In developing the above criterion based on the capillary number, the contact-line singularity is not important because the capillary numbers are calculated using experimentally determined parameters (e.g., contact angle, contact-line speed, shear rate, etc).

For a nonionic surfactant solution based on dioctyl sulfosuccinate sodium salt on a hydrophobic flat surface, Bonn and coworkers showed that spreading dynamics is similar to that of the Newtonian fluid for concentrations beyond critical micelle concentration (CMC) [66]. However, for a dilute surfactant solution based on trisiloxane, the spreading occurs much more rapidly than a Newtonian fluid with the droplet radius varying as $R(t) \propto t^{\alpha}$ with α taking all values between 0.1 and 1 [67]. The latter surfactant system is a peculiar solution known to exhibit superspreading behavior [66,68]. The super spreading behavior has been linked to several mechanisms including (1) caterpillar motion of the contact line that reduces the viscous dissipation [69], (2) transfer of surfactant molecules from air-liquid to the liquid-solid interface [70], (3) formation of surfactant aggregates at the fluid contact line [71] and (4) Marangoni flows due to depletion of the surfactant at the leading edge of the contact line [72]. Since super spreading is not observed in our experiments, the above mechanisms do not affect the measurements reported in this study.

Additionally, surfactant adsorption to the liquid-air or liquid-solid interfaces could deplete the droplet interior of the surfactant and as a result affect droplet spreading dynamics. For example, von Bahr *et al.* [73] showed that for Thiohexadecanol surfactant solutions in the vicinity of CMC, the adsorption of surfactant to the interfaces is important and leads to $R(t) \propto t^{1/2}$. In the experiments reported in this paper the fluid spreading rate is much slower than the one noted by von Bahr *et al.* [73]. In addition, the surfactant concentrations are much higher than their CMC ($>10^3$). Therefore, we expect that the adsorption of surfactant molecules to the liquid-vapor and liquid-solid interfaces should not affect the concentration of surfactants in the bulk and consequently, surfactant solutions spreading dynamics will not be influenced by adsorption of surfactants to such interfaces.

Finally, the droplet spreading on heterogeneous or rough substrates maybe affected by the pinning-depinning phenomenon, where the leading edge of the contact line exhibits a stick-slip

pattern [74,75]. Our measurements of the radius of the contact line presented in Fig. 8 do not show any signs of stick-slip behavior. In fact, the high spatial and temporal resolutions (10 μm and 1 ms) of our visualization technique would have enabled us to detect the pinning-depinning phenomenon at the contact line if it had existed. We have also presented new videos that show the filament thinning and contact-line spreading dynamics (see Supplemental Material videos [56]). As a result, we believe that the pinning-depinning mechanism does not play any role in our DoS experiments with the large substrate. A systematic investigation of the effect of surface roughness on wetting dynamics in DoS experiments is beyond the scope of this work and we hope to present such results in the near future.

VI. CONCLUSIONS AND OUTLOOK

Harking back to the motivation of this study, we investigated for the first time the link between fluid wetting and the filament pinch-off dynamics in model viscoelastic surfactant solutions over a wide range of salt concentrations. The key findings of this study include the following: First, we identified two new flow regimes which have not been previously reported in prior pertaining literature on complex fluids [13,37–41]. In regime I, the extensional flow is not affected by motion of the contact line on the solid substrate, while, in regime II, the motion of the fluid contact line on the big solid substrate significantly impacts the extensional flow properties by shortening the filament lifetimes, extensional relaxation times, and the maximum Trouton ratios of the fluids compare to that of the pinned contact line. Second, we analyzed the wetting and spreading dynamics of these viscoelastic systems by measuring the contact-line radius and the contact angle, and illustrated that the spreading dynamics of these viscoelastic fluids is controlled by a combination of wetting forces and viscous dissipation. This is perhaps unsurprising because the characteristic shear rates at the moving fluid contact line are close to Newtonian regime when compared to the steady shear rheology data; a result that renders the effects of shear thinning and elasticity negligible. Third, we developed, for the first time, a criterion based on the dimensionless capillary number that is capable of distinguishing these two flow regimes from each other. This criterion also holds for Newtonian fluids. This study confirms our hypothesis that wetting dynamics and extensional flow properties of complex fluids are closely linked to each other.

In future, we will systematically investigate the link between wetting dynamics and extensional flow properties of a wide range of complex fluids including polymer solutions, polyelectrolytes, yield stress fluids, colloidal suspensions, among others. In particular, it will be interesting to test if the same criterion based on the capillary number can explain the interplay between wetting dynamics and extensional flows in other types of complex fluids. Finally, the wetting dynamics on solid substrates depends on the type (hydrophilic versus hydrophobic) and roughness of the substrate. A systematic investigating of the effects of surface type and roughness on filament pinch-off dynamics of viscoelastic surfactant solutions is currently underway.

[1] P.-G. De Gennes, Wetting: Statics and dynamics, Rev. Mod. Phys. **57**, 827 (1985).
[2] D. Bonn, J. Eggers, J. Indekeu, J. Meunier, and E. Rolley, Wetting and spreading, Rev. Mod. Phys. **81**, 739 (2009).
[3] G. Lu, X.-D. Wang, and Y.-Y. Duan, A critical review of dynamic wetting by complex fluids: From Newtonian fluids to non-Newtonian fluids and nanofluids, Adv. Colloid Interface Sci. **236**, 43 (2016).
[4] S. Kumar, Liquid transfer in printing processes: Liquid bridges with moving contact lines, Annu. Rev. Fluid Mech. **47**, 67 (2015).
[5] J. N. Israelachvili, *Intermolecular and Surface Forces* (Academic Press, San Diego, 2011).
[6] L. M. Walker, Rheology and structure of worm-like micelles, Curr. Opin. Colloid Interface Sci. **6**, 451 (2001).

[7] J. Yang, Viscoelastic wormlike micelles and their applications, Curr. Opin. Colloid Interface Sci. **7**, 276 (2002).
[8] C. A. Dreiss, Wormlike micelles: Where do we stand? Recent developments, linear rheology and scattering techniques, Soft Matter **3**, 956 (2007).
[9] B. Yesilata, C. Clasen, and G. H. McKinley, Nonlinear shear and extensional flow dynamics of wormlike surfactant solutions, J. Non-Newtonian Fluid Mech. **133**, 73 (2006).
[10] A. Bhardwaj, E. Miller, and J. P. Rothstein, Filament stretching and capillary breakup extensional rheometry measurements of viscoelastic wormlike micelle solutions, J. Rheol. **51**, 693 (2007).
[11] R. Omidvar, A. Dalili, A. Mir, and H. Mohammadigoushki, Exploring sensitivity of the extensional flow to wormlike micellar structure, J. Non-Newtonian Fluid Mech. **252**, 48 (2018).
[12] D. Sachsenheimer, C. Oelschlaeger, S. Müller, J. Küstner, Sebastian Bindgen, and Norbert Willenbacher, Elongational deformation of wormlike micellar solutions, J. Rheol. **58**, 2017 (2014).
[13] R. Omidvar, S. Wu, and H. Mohammadigoushki, Detecting wormlike micellar microstructure using extensional rheology, J. Rheol. **63**, 33 (2019).
[14] M. Chellamuthu and J. P. Rothstein, Distinguishing between linear and branched wormlike micelle solutions using extensional rheology measurements, J. Rheol. **52**, 865 (2008).
[15] J. P. Rothstein, Transient extensional rheology of wormlike micelle solutions, J. Rheol. **47**, 1227 (2003).
[16] S. M. Recktenwald, S. J. Haward, A. Q. Shen, and W. Norbert, Heterogeneous flow inside threads of low viscosity fluids leads to anomalous long filament lifetimes, Sci. Rep. **9**, 7110 (2019).
[17] H. Mohammadigoushki and S. J. Muller, Sedimentation of a sphere in wormlike micellar fluids, J. Rheol. **60**, 587 (2016).
[18] S. Chen and J. P. Rothstein, Flow of a wormlike micelle solution past a falling sphere, J. Non-Newtonian Fluid Mech. **116**, 205 (2004).
[19] J. A. Pathak and S. D. Hudson, Rheo-optics of equilibrium polymer solutions: Wormlike micelles in elongational flow in a microfluidic cross-slot, Macromolecules **39**, 8782 (2006).
[20] S. J. Haward, T. J. Ober, M. S. N. Oliveira, M. A. Alves, and G. H. McKinley, Extensional rheology and elastic instabilities of a wormlike micellar solution in a microfluidic cross-slot device, Soft Matter **8**, 536 (2012).
[21] N. Dubash, P. Cheung, and A. Q. Shen, Elastic instabilities in a microfluidic cross-slot flow of wormlike micellar solutions, Soft Matter **8**, 5847 (2012).
[22] P. F. Salipante, S. E. Meek, and S. D. Hudson, Flow fluctuations in wormlike micelle fluids, Soft Matter **14**, 9020 (2018).
[23] G. R. Moss and J. P. Rothstein, Flow of wormlike micelle solutions past a confined circular cylinder, J. Non-Newtonian Fluid Mech. **165**, 1505 (2010).
[24] A. A. Dey, Y. Modarres-Sadeghi, and J. P. Rothstein, Viscoelastic fluid-structure interactions between a flexible cylinder and wormlike micelle solution, Phys. Rev. Fluids **3**, 063301 (2018).
[25] Y. Zhao, A. Q. Shen, and S. J. Haward, Flow of wormlike micellar solutions around confined microfluidic cylinders, Soft Matter **12**, 8666 (2016).
[26] S. Wu and H. Mohammadigoushki, Sphere sedimentation in wormlike micelles: Effect of micellar relaxation spectrum and gradients in micellar extensions, J. Rheol. **62**, 1061 (2018).
[27] S. Wu and H. Mohammadigoushki, Flow of a model shear-thickening micellar fluid past a falling sphere, Phys. Rev. Fluids **4**, 073303 (2019).
[28] H. Mohammadigoushki and S. J. Muller, Creeping flow of a wormlike micelle solution past a falling sphere: Role of boundary conditions, J. Non-Newtonian Fluid Mech. **257**, 44 (2018).
[29] L. Leger and J. F. Joanny, Liquid spreading, Rep. Prog. Phys. **55**, 431 (1992).
[30] T. D. Blake, The physics of moving wetting lines, J. Colloid Interface Sci. **299**, 1 (2006).
[31] S. Rafaï, D. Bonn, and A. Boudaoud, Spreading of non-Newtonian fluids on hydrophilic surfaces, J. Fluid Mech. **513**, 77 (2004).
[32] X. D. Wang, Y. Zhang, D. J. Lee, and X. F. Peng, Spreading of completely wetting or partially wetting power-law fluid on solid surface, Langmuir **23**, 9258 (2007).
[33] J. Han and C. Kim, Spreading of Boger fluid on horizontal surface, J. Non-Newtonian Fluid Mech. **202**, 120 (2013).

[34] Y. Wei, G. K. Seevaratnam, S. Garoff, E. Rame, and L. M. Walker, Dynamic wetting of Boger fluids, J. Colloid Interface Sci. **313**, 274 (2007).
[35] Q. Min, Y.-Y. Duan, X.-D. Wang, Z.-P. Liang, D.-J. Lee, and A. Su, Spreading of completely wetting, non-Newtonian fluids with non-power-law rheology, J. Colloid Interface Sci. **348**, 250 (2010).
[36] J. Dinic, L. N. Jimenez, and V. Sharma, Pinch-off dynamics and dripping-onto-substrate (dos) rheometry of complex fluids, Lab Chip **17**, 460 (2017).
[37] J. Dinic and V. Sharma, Macromolecular relaxation, strain, and extensibility determine elastocapillary thinning and extensional viscosity of polymer solutions, Proc. Natl. Acad. Sci. USA **116**, 8766 (2019).
[38] J. Dinic, Y. Zhang, L. N. Jimenez, and V. Sharma, Extensional relaxation times of dilute, aqueous polymer solutions, ACS Macro Lett. **4**, 804 (2015).
[39] S. Sur and J. Rothstein, Drop breakup dynamics of dilute polymer solutions: Effect of molecular weight, concentration, and viscosity, J. Rheol. **62**, 1245 (2018).
[40] M. Rosello, S. Sur, B. Barbet, and J. P. Rothstein, Dripping-onto-substrate capillary breakup extensional rheometry of low-viscosity printing inks, J. Non-Newtonian Fluid Mech. **266**, 160 (2019).
[41] K. A. Marshall, A. M. Liedtke, A. H. Todt, and T. W. Walker, Extensional rheometry with a handheld mobile device, Exp. Fluids **58**, 69 (2017).
[42] L. H. Tanner, The spreading of silicone oil drops on horizontal surfaces, J. Phys. D: Appl. Phys. **12**, 1473 (1979).
[43] R. L. Hoffman, A study of the advancing interface. I. Interface shape in liquid-gas systems, J. Colloid Interface Sci. **50**, 228 (1975).
[44] O. V. Voinov, Hydrodynamics of wetting, Fluid Dyn. **11**, 714 (1976).
[45] R. G. Cox, The dynamics of the spreading of liquids on a solid surface. part 1. Viscous flow, J. Fluid Mech. **168**, 169 (1986).
[46] V. M. Starov, A. N. Tyatyushkin, M. G. Velarde, and S. A. Zhdanov, Spreading of non-Newtonian liquids over solid substrates, J. Colloid Interface Sci. **257**, 284 (2003).
[47] V. Croce, T. Cosgrove, G. Maitland, T. Hughes, and G. Karlsson, Rheology, cryogenic transmission electron spectroscopy, and small-angle neutron scattering of highly viscoelastic wormlike micellar solutions, Langmuir **19**, 8536 (2003).
[48] S. R. Raghavan, G. Fritz, and E. W. Kaler, Wormlike micelles formed by synergistic self-assembly in mixtures of anionic and cationic surfactants, Langmuir **18**, 3797 (2002).
[49] D. P. Acharya, K. Hattori, T. Sakai, and H. Kunieda, Phase and rheological behavior of salt-free alkyltrimethylammonium bromide/alkanoyl-n-methylethanolamide/water systems, Langmuir **19**, 9173 (2003).
[50] A. Aït Ali and R. Makhloufi, Linear and nonlinear rheology of an aqueous concentrated system of cethyltrimethylammonium chloride and sodium salicylate, Phys. Rev. E **56**, 4474 (1997).
[51] Z. Lin, Branched worm-like micelles and their networks, Langmuir **12**, 1729 (1996).
[52] C. Oelschlaeger, M. Schopferer, F. Scheffold, and N. Willenbacher, Linear-to-branched micelles transition: A rheometry and diffusing wave spectroscopy study, Langmuir **25**, 716 (2009).
[53] T. Imae and T. Kohsaka, Size and electrophoretic mobility of tetradecyltrimethylammonium salicylate (C14TASal) micelles in aqueous media, J. Phys. Chem. **96**, 10030 (1992).
[54] L. Ziserman, L. Abezgauz, O. Ramon, S. R. Raghavan, and D. Danino, Origins of the viscosity peak in wormlike micellar solutions. 1. Mixed catanionic surfactants: A cryo-transmission electron microscopy study, Langmuir **25**, 10483 (2009).
[55] L. J. Magid, The surfactant-polyelectrolyte analogy, J. Phys. Chem. B **102**, 4064 (1998).
[56] See Supplemental Material at http://link.aps.org/supplemental/10.1103/PhysRevFluids.5.053303 for image analysis technique for the wetting process (Fig. 1), steady-state shear viscosity (Fig. 2), small amplitude oscillatory shear rheology (Fig. 3), contact-line radius as a function of time (Fig. 4), first normal stress difference (Fig. 5) for sample wormlike micellar solutions; midfilament diameter (Fig. 6), rheological and physical properties (Table I), and radius as a function of time (Fig. 7) for two Newtonian fluids.
[57] V. M. Entov and E. J. Hinch, Effect of a spectrum of relaxation times on the capillary thinning of a filament of elastic liquid, J. Non-Newtonian Fluid Mech. **72**, 31 (1997).

[58] A. M. Cazabat and M. A. C. Stuart, Dynamics of wetting: Effects of surface roughness, J. Phys. Chem. **90**, 5845 (1986).
[59] J.-D. Chen, Experiments on a spreading drop and its contact angle on a solid, J. Colloid Interface Sci. **122**, 60 (1988).
[60] J.-D. Chen and N. Wada, Wetting Dynamics of the Edge of a Spreading Drop, Phys. Rev. Lett. **62**, 3050 (1989).
[61] Y. Wang, D.-Q. Minh, and G. Amberg, Dynamic wetting of viscoelastic droplets, Phys. Rev. E **92**, 043002 (2015).
[62] C. Huh and L. E. Scriven, Hydrodynamic model of steady movement of a solid/liquid/fluid contact line, J. Colloid Interface Sci. **35**, 85 (1971).
[63] Y. D. Shikhmurzaev, The moving contact line on a smooth solid surface, Int. J. Multiphase Flow **19**, 589 (1993).
[64] D. E. Weidner and L. W. Schwartz, Contact-line motion of shear-thinning liquids, Phys. Fluids **6**, 3535 (1994).
[65] A. Carre and P. Woehl, Hydrodynamic behavior at the triple line of spreading liquids and the divergence problem, Langmuir **18**, 3600 (2002).
[66] S. Rafaï and D. Bonn, Spreading of non-Newtonian fluids and surfactant solutions on solid surfaces, Physica A: Stat. Mech. Appl. **358**, 58 (2005).
[67] S. Rafai, D. Sarker, V. Bergeron, J. Meunier, and D. Bonn, Superspreading: Aqueous surfactant drops spreading on hydrophobic surfaces, Langmuir **18**, 10486 (2002).
[68] J. Venzmer and S. P. Wilkowski, *Trisiloxane Surfactants—Mechanisms of Spreading and Wetting* (John Wiley Sons, New York, NY, 2008), Chap. 111, pp. 690–698.
[69] V. Starov, Static contact-angle hysteresis on smooth, homogeneous solid substrates, Colloid Polym. Sci. **291**, 261 (2013).
[70] G. Karapetsas, R. V. Craster, and O. K. Matar, On surfactant-enhanced spreading and superspreading of liquid drops on solid surfaces, J. Fluid Mech. **670**, 5 (2011).
[71] H. A. Ritacco, F. Ortega, R. G. Rubio, N. Ivanova, and V. M. Starov, Equilibrium and dynamic surface properties of trisiloxane aqueous solutions: Part 1. Experimental results, Colloids Surf., A **365**, 199 (2010).
[72] A. Chengara, A. Nikolov, and D. Wasan, Surface tension gradient driven spreading of trisiloxane surfactant solution on hydrophobic solid, Colloids Surf., A **206**, 31 (2002).
[73] M. von Bahr, F. Tiberg, and B. V. Zhmud, Spreading dynamics of surfactant solutions, Langmuir **15**, 7069 (1999).
[74] Y. V. Kalinin, V. Berejnov, and R. E. Thorne, Contact-line pinning by microfabricated patterns: Effects of microscale topography, Langmuir **25**, 5391 (2009).
[75] Q. Li, P. Zhou, and H. J. Yan, Pinning–depinning mechanism of the contact line during evaporation on chemically patterned surfaces: A lattice Boltzmann study, Langmuir **32**, 9389 (2016).